Chapter 11 General Circulation Modeling

The *general circulation* of the atmosphere can be defined as the totality of motions that characterize the global-scale atmospheric flow. Since many of the eddy motions in the middle atmosphere have their origins in the troposphere, it is not possible to isolate the general circulation of the middle atmosphere from that of the atmosphere as a whole. The problem of modeling the general circulation is one of numerically simulating the global circulation of the atmosphere using the primitive equations, with only a minimum of assumptions and parameterizations. Ideally, only the external conditions (solar radiation, sea surface temperature, and permanent ice cover) should be specified and the model should self-consistently compute the temperature, wind, cloud, and trace species distributions as functions of three-dimensional space and time. In practice, at the present stage of model development, many compromises are necessary both for scientific reasons and for reasons of computational efficiency.

General circulation models (GCMs) can provide stringent tests of our understanding of the atmospheric system. If all relevant physical processes are correctly represented, then a GCM should provide a faithful simulation of the three-dimensional circulation. Thus, one of the primary roles of the GCM in middle atmosphere research is as an "experimental" tool to test the adequacy of our understanding of various physical processes. Externally specified parameters (e.g., orography) can be altered to provide "controlled" experiments that cannot be done on the real atmosphere. Deficiencies in model simulations can provide indications that important processes have been omitted or inadequately treated (see the discussion of the cold polar bias in Section 11.2.1).

A long-term objective of middle atmosphere GCM research is to develop simulations of the atmosphere that are suitable for use in predicting possible anthropogenic perturbations of the ozone layer. Although completely interactive radiative-chemical-dynamical models suitable for such predictions are not yet available, general circulation models have in the past several years provided many fundamental dynamical insights as well as information on the interaction of radiation and dynamics. To date comparatively little general circulation model research has been devoted to the subtle problems of chemical-dynamical interactions, although wind "data" from GCM simulations have been used in studies of trace constituent transport. There is little doubt, however, that GCMs are the most powerful technique available for developing an understanding of the full range of radiative, dynamical, and chemical interactions in the middle atmosphere. These models also offer perhaps the best methodology for elucidating the dynamical interactions between the troposphere and stratosphere, both for assessing the influence of the middle atmosphere on the climate of the troposphere and for studying the driving of the middle atmosphere by the circulation of the troposphere.

The overwhelming majority of general circulation model studies have been devoted to the tropospheric climate problem. Most general circulation models do, however, include at least the lower stratosphere in order to avoid problems that would result from imposing a rigid-lid upper boundary condition at the tropopause. Such models have been used to investigate various aspects of the stratospheric circulation, including sudden stratospheric warmings. In fact, the ability of a given model to generate realistic midwinter warmings has often been taken as a key test of its suitability for stratospheric studies.

Efforts to model the bulk of the middle atmosphere are in a much less mature state than is tropospheric general circulation modeling. The very large demands on computer resources required for multilevel models extending over many scale heights in altitude have forced middle atmosphere modelers to make a number of simplifications. For example, some models have been based on quasi-geostrophic dynamics, some have included only a single hemisphere, some have used greatly simplified radiative heating algorithms, and some have featured highly simplified tropospheres.

The primary focus in this chapter will be on those models that can be regarded as true general circulation models. By this, we mean primitive equation models that attempt to simulate the entire global atmosphere with horizontal resolution adequate to resolve synoptic-scale eddies, and with radiative processes calculated from accurate radiative transfer codes. However, we shall also mention some models that, while not meeting all these

criteria, have provided important insights into the dynamics of the middle atmosphere.

11.1 Models of the Lower Stratosphere

The first primitive-equation general circulation model that attempted to resolve the lower stratosphere was that of Smagorinsky *et al.* (1965), developed at the Geophysical Fluid Dynamics Laboratory (GFDL). This model had nine prediction levels in the vertical, with the top three levels at standard heights of 12, 18, and 31.6 km. The horizontal domain was limited to the Northern Hemisphere and represented by a rectangular grid on a polar stereographic map. In this model, as in some subsequent GFDL models, the solar radiation was set at its annual mean value. The hydrological cycle was also omitted and the lower boundary was taken to be a uniform land surface with zero heat capacity. The radiatively active constituents (ozone, water vapor, carbon dioxide, and clouds) were all assigned zonally and annually averaged climatological mean values.

A model without topography could hardly be expected to generate vertically propagating planetary waves of sufficient strength to properly account for the eddy forcing required to satisfy the zonal mean climatology of the winter stratosphere (cf. Chapter 7). Nevertheless, the Smagorinsky model did at least qualitatively simulate the zonal mean temperature distribution in the lower stratosphere, the high cold tropical tropopause, and the low polar tropopause. However, there was also a notable deficiency: the polar stratospheric temperatures were significantly lower than the observed annual mean values, and (in agreement with the thermal wind balance) the mean zonal wind was significantly stronger than in the observed annual mean.

Manabe and Hunt (1968) used a model similar in structure to that of Smagorinsky *et al.* (1965), but with 18 levels in the vertical extending from the surface to 37.5 km altitude. The computed zonal mean temperatures and winds for this model were in better agreement with observations than were those for the Smagorinsky model. However, the polar cold bias remained. In fact, the computed polar temperature distribution agreed better with the observed winter mean than with the observed annual mean, even though annual mean radiative forcing was used.

The Manabe and Hunt experiments showed that increased vertical resolution in the stratosphere can improve the stratospheric simulation. Nevertheless, the incorporation of annual mean radiative forcing, the absence of topography, the restriction of the model domain to a single hemisphere, and other model limitations prevented the model from fully simulating important aspects of the circulation of the stratosphere.

In recent years several groups have formulated global general circulation models that have incorporated realistic topography and have at least crudely resolved the lower stratosphere. In most cases, these models have utilized the "sigma" coordinate system, in which the vertical coordinate is defined as $\sigma = p/p^*$, where $p^*(x, y, t)$ is the surface pressure. This system has the advantage that the coordinate surface $\sigma = 1$ coincides with the earth's surface everywhere, so that the lower boundary condition becomes simply $D\sigma/Dt = 0$. The discretization of the equations in the horizontal has commonly been in the form of finite differencing on a spherical grid with typically about 5° to 10° latitude and longitude grid spacing. Spectral transform models have become popular. A well-known example of a spectral model is the Community Climate Model (CCM) of the National Center for Atmospheric Research (NCAR), which is based on expansion in spherical harmonics with truncation typically at wave number 15.

The details of the physical parameterizations used in the various models differ, but they tend to share certain common features:

1. Sea surface temperatures are externally specified using observed climatological values. In some models these are specified to vary according to the annual cycle, but in many cases either annual means or fixed January monthly means are used. Surface temperatures over land are computed from a surface energy-balance equation.
2. Boundary-layer fluxes of momentum, heat, and moisture are parameterized by the *bulk aerodynamic method.* In this method the flux for each of these fields is specified to be proportional to the magnitude of the horizontal wind at the lowest model level times the difference between the value of the field at the boundary and the lowest model level.
3. Sub-grid-scale horizontal mixing is usually parameterized either by nonlinear diffusion or by second- or fourth-order linear diffusion; occasionally mathematical filtering is employed.
4. The hydrological cycle is included, with predicted water vapor and precipitation explicitly determined for forced synoptic-scale uplift, and parameterized for convective overturning.
5. Radiative heating and cooling by both solar and longwave radiation are computed using parameterized versions of the radiative transfer equations. Specified zonally averaged distributions of the radiatively active constituents are often used. Some models (e.g., the CCM) do, however, compute cloud-radiation effects interactively using the zonally varying cloudiness predicted by the model.

Despite the many improvements that have been made in general circulation model simulations in the past several years, the cold polar winter stratosphere bias has remained as an almost universal model deficiency.

Although it has sometimes been suggested that the cold bias is due simply to poor vertical resolution or to problems associated with the upper boundary condition, the problem remains even in the GFDL "SKYHI" model, which has excellent vertical resolution and an upper boundary near the mesopause.

There are basically only two plausible sources for the cold bias—radiative and dynamical. Radiative sources of the bias could involve either errors in the computed radiative cooling rates for given departures from the radiatively determined temperature, or errors in the radiatively determined temperature itself (i.e., in the temperature that would be computed in the model in the absence of dynamical heating; see Section 7.1). Dynamical sources of the cold bias could include problems in representation of eddy sources and sinks for either large- or small-scale eddies so that the net dynamical heating is underestimated and, as a consequence, the simulated winter stratospheres are too close to radiative equilibrium.

It is certainly true that radiative cooling computations for the winter stratosphere must be done with great care. Seemingly small differences in parameterizations of the radiative effects can produce rather large differences in the model climatology, as has been pointed out by Ramanathan *et al.* (1983). They showed that the NCAR CCM was able to produce a greatly improved winter lower stratosphere simulation when certain seemingly minor changes were made in the treatment of both solar and longwave radiation. These included the following:

1. Careful treatment of the upper boundary condition for solar heating by ozone.
2. Inclusion of correct temperature dependence for the 15-μm CO_2 band.
3. A reduction in the assumed H_2O mixing ratio in the polar stratosphere.
4. Allowance for variable cirrus-cloud emissivity dependent on the cloud water content.

Simulations using this improved radiation package for January mean conditions were compared with simulations using the same dynamics, but the earlier radiation code. As shown in Fig. 11.1, the new radiation code resulted in a remarkably improved simulation of the climate. The tropospheric subtropical and stratospheric polar night jets were well separated, in agreement with observations (Figs. 1.4 and 5.2), and the polar temperatures were in good agreement with those observed (Figs. 1.3 and 5.1).

Although these results might tempt one to conclude that better modeling of the radiative forcing is the key to improved simulations of the middle atmosphere, the actual situation is not so simple. The large differences between the two simulations shown in Fig. 11.1 cannot be attributed to radiation alone. In the polar stratosphere the temperature difference between

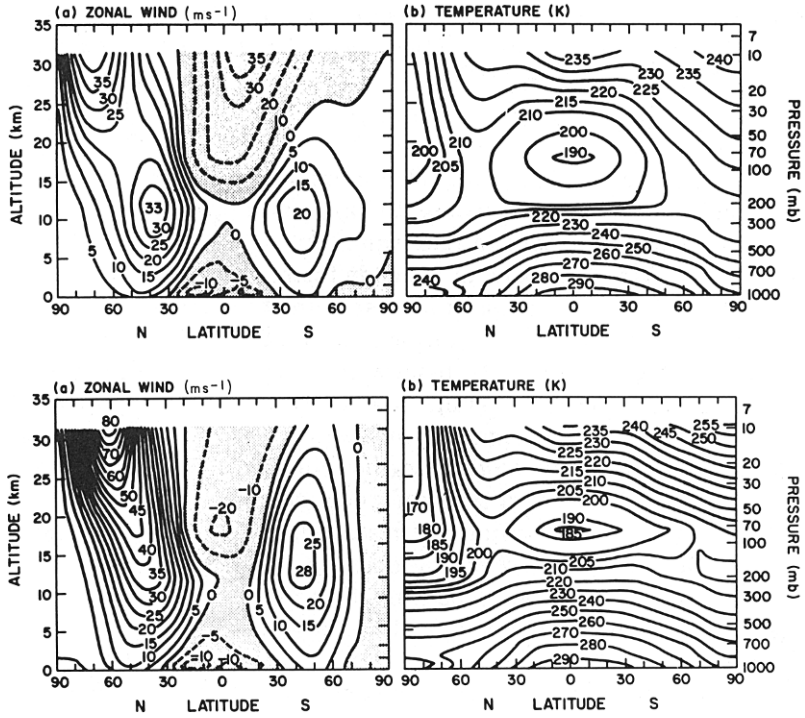

Fig. 11.1. Mean zonal winds ($m\,s^{-1}$) and zonally averaged temperatures in the NCAR CCM with improved (top) and degraded (bottom) radiation algorithms. [After Ramanathan *et al.* (1983). American Meteorological Society.]

the two cases shown in Fig. 11.1 is about three times the amount that can be attributed to direct effects of changes in the radiation code (i.e., to changes in the radiative equilibrium temperature distribution, and in cooling rates for a given departure from radiative equilibrium). The remaining difference must be due to an increase in the eddy forcing, which results in a much greater dynamical heating in the simulation with the improved radiation scheme. Thus, not only is the radiative equilibrium temperature somewhat warmer in the model with the improved radiative code, but the eddies have a different structure so that the departure from radiative equilibrium is maintained at a considerably higher value than in the original version.

We must conclude that a satisfactory simulation of the winter polar stratosphere is only possible if the model produces sufficient eddy forcing to maintain the required departure from radiative equilibrium. The distribution of eddy forcing required to maintain a given radiative heating rate can

be estimated (within quasi-geostrophic theory) by taking the time average of Eq. (3.5.7) or Eq. (7.2.4c):

$$(\nabla \cdot \mathbf{F} + \rho_0 \bar{X})_y = (\rho_0 f_0 \bar{Q}/\bar{\theta}_{0z})_z. \tag{11.1.1}$$

The heating rate $\bar{Q}$ is approximately proportional to the deviation of $\bar{\theta}$ from its radiative equilibrium value $\bar{\theta}_r$. Thus, from Eq. (11.1.1) the magnitude of the departure from radiative equilibrium is approximately linearly proportional to the magnitude of the eddy forcing. The precise form of the eddy forcing is not important for the present argument. Either the Eliassen-Palm (EP) flux divergence due to the resolved eddies or the zonal mean drag due to parameterized small-scale eddies can provide the required forcing. It is only necessary that the *total* forcing be sufficient in amplitude.

That the *amount* rather than the *form* of the eddy forcing is the key to simulating a realistic climatology in the winter stratosphere was shown nicely by Boville (1985) in a series of simulations using a 14-level version of the NCAR CCM with improved resolution in the lower stratosphere. Now, Eq. (3.6.5) indicates that in a time mean the EP flux divergence is proportional to the wave damping if nonlinear effects can be neglected. In the CCM both radiative damping and mechanical (diffusive) damping are present. Boville showed that the magnitude of the EP flux divergence was approximately proportional to the product of the square of the wave amplitude and the inverse time scale for radiative plus mechanical damping. In this model, as in most GCMs, the amplitude of the stationary planetary waves simulated in the winter stratosphere was less than observed in the atmosphere. Thus, a larger damping rate was required to produce the same amount of EP flux divergence as in the atmosphere. Boville showed by controlled experiments that the parameterized momentum diffusion in the CCM (which provides wave damping at about the same rate as the computed radiative damping, and also directly damps the zonal mean flow) was essential for simulating a realistic climatology. Omission of the mechanical damping resulted in a smaller total EP flux divergence, and hence the temperatures became closer to radiative equilibrium unless the radiative damping of the eddies was artifically enhanced. Increasing the damping rate in the stratosphere does, however, reduce the propagation of wave activity into the mesosphere; thus alone it cannot improve the simulation throughout the entire middle atmosphere.

If the model were to produce larger-amplitude planetary waves, then it is conceivable that radiative wave damping could provide a sufficient amplitude of EP flux divergence to maintain the observed zonal mean temperature distribution. Present indications are, however, that some mechanical dissipation by small scale motions must be present in the stratosphere, and for the

mesosphere there is little doubt that gravity wave breaking must be a dominant factor in the momentum balance.

11.2 The GFDL SKYHI model

The general circulation model that currently provides the most complete representation of the middle atmosphere is the SKYHI model, developed at GFDL (Fels *et al.*, 1980). This model has 40 prediction levels extending from the surface of the earth to about the 80 km level. The vertical coordinate system, shown schematically in Fig. 11.2, is a hybrid system in which the sigma surfaces are defined as

$$\sigma = \frac{p - p_c}{p^* - p_c}, \qquad p > p_c; \qquad \sigma = \frac{p - p_c}{1013.25 - p_c}, \qquad p < p_c$$

where $p^*(x, y, t)$ is the surface pressure and $p_c = 353.55$ mb. Thus, the coordinates are equivalent to the usual terrain-following σ coordinates below about 350 mb and become isobaric coordinates above that level. The vertical spacing of prediction levels increases gradually from the surface to the top boundary; it is about 1 km standard height in the midtroposphere and about 3 km at the stratopause. The horizontal grid mesh is based on spherical coordinates with Fourier filtering (i.e., removal of the high zonal wave-number components) near the poles. In early experiments a rather coarse resolution of 9° latitude by 10° longitude was employed. More recent experiments have employed versions with 5° by 6°, 3° by 3.6°, and even 1° by 1.2° resolution.

The treatment of physical processes in the troposphere is more extensive than in the early GFDL models. The model includes topography, realistic distributions of continents and oceans, and a hydrological cycle. Predicted fields include the wind, temperature, water vapor, ground temperature, soil moisture, snow cover, and surface pressure. However, cloudiness, pack ice, and ocean surface temperatures are all externally specified using climatological mean data.

The radiative heating and cooling is calculated once every 12 hr using diurnally averaged solar insolation. The solar heating in the middle atmosphere is based on the parameterization of Lacis and Hansen (1974), which includes heating by ozone and molecular oxygen. The infrared atmospheric radiation is computed using the scheme of Fels and Schwarzkopf (1981). A zonally averaged ozone distribution is specified from the surface to 34 km; above that level, temperature-dependent photochemistry is included by allowing the ozone to deviate from a specified climatological mean in response to temperature fluctuations, using a temperature-dependent parameterization of the photochemical equilibrium.

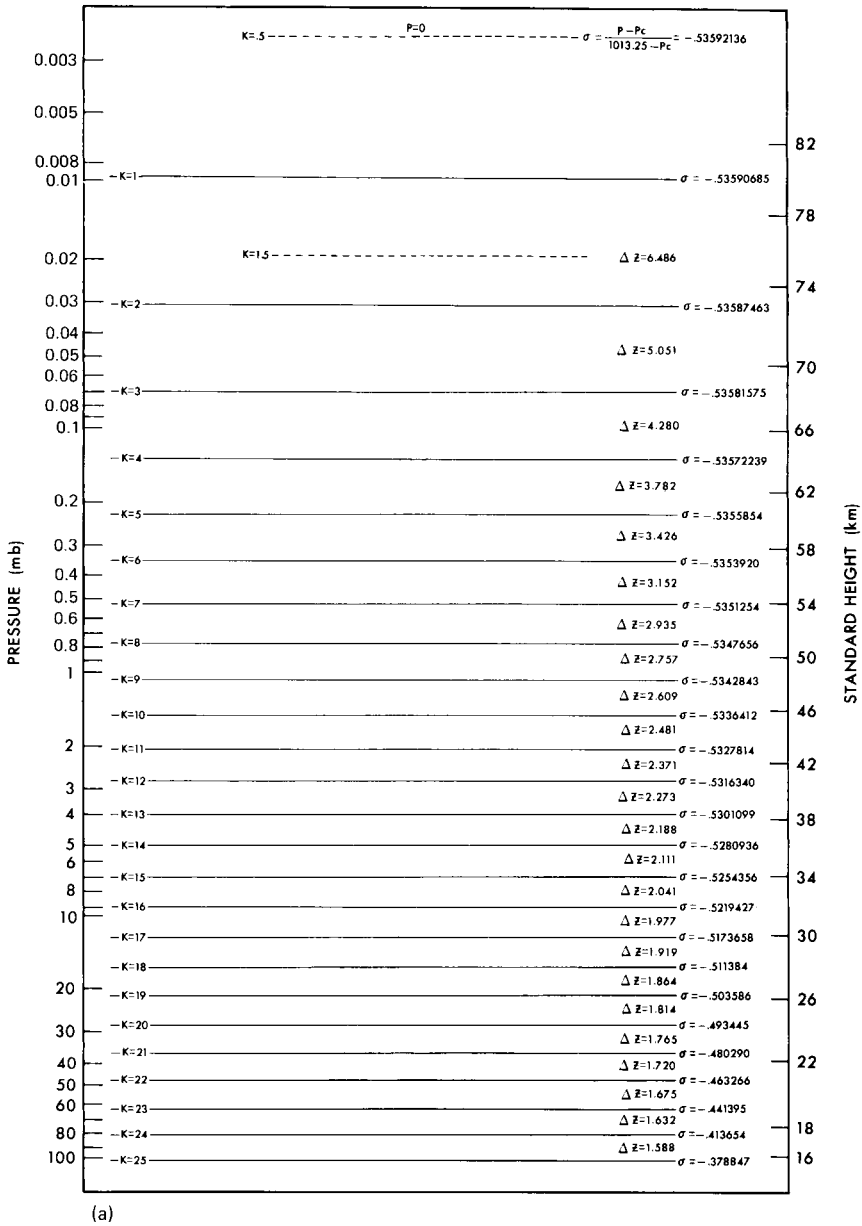

Fig. 11.2. (a) Upper and (b) lower portions of the SKYHI model's vertical coordinate system. The standard height labeling is based on a midlatitude standard atmosphere temperature distribution. [After Fels *et al.* (1980). American Meteorological Society.] *Figure continues.*

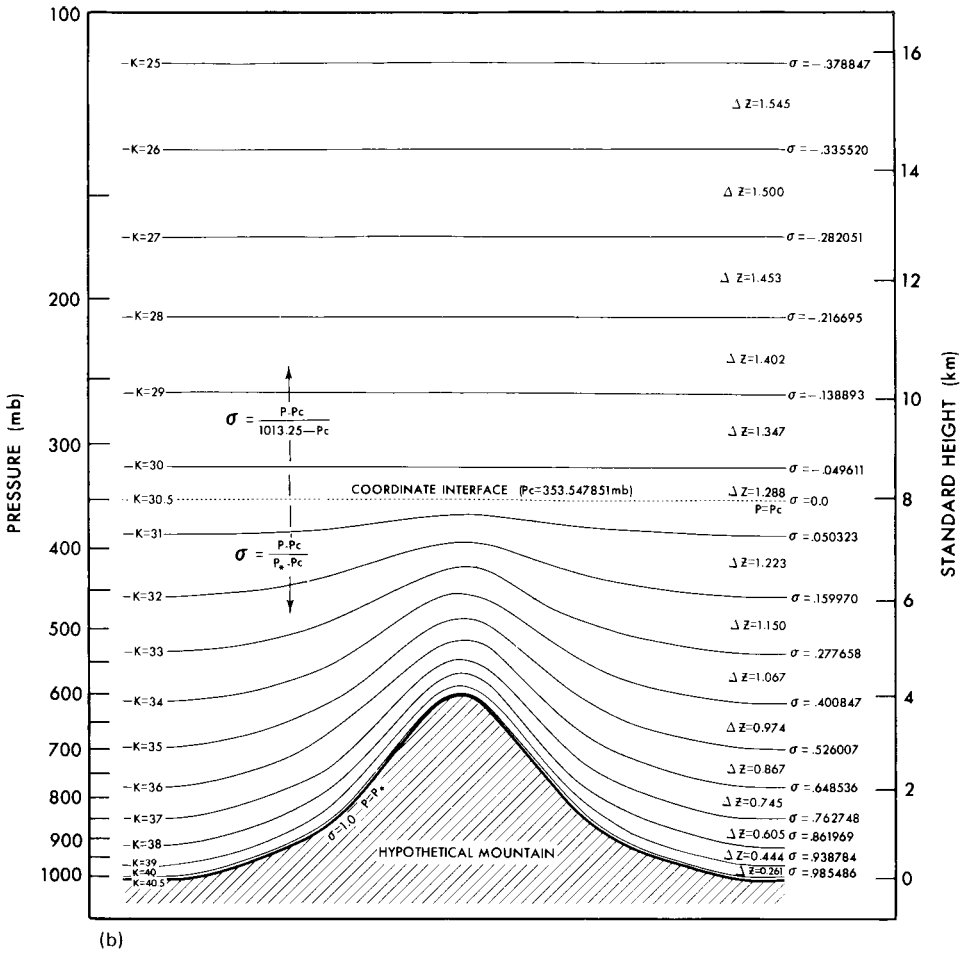

Fig. 11.2 (*continued*)

11.2.1 The Cold Winter Pole

The SKYHI model has provided useful information on the possible causes of the winter polar cold bias discussed in the previous section. Experiments with an annual average radiation version of the model have demonstrated that the polar cold bias does not disappear when high vertical resolution and a high-altitude upper boundary are used. In fact, the cold bias turns out to be a bigger problem in this model than in models with upper boundaries in the stratosphere. This should not be surprising, since, as discussed in Chapter 7, it is believed that gravity-wave drag and diffusion

play primary roles in the momentum balance of the mesosphere. There is no parameterization of gravity-wave drag in the SKYHI model, and the experiments with horizontal resolutions of about 9°, 5°, and 3° are all too coarse to resolve the several-hundred-kilometer horizontal wavelength internal gravity waves that appear to be the primary breaking waves in the extratropics. Early results from a 1° resolution model, which can resolve the longer gravity waves, indicate that the extra dynamical heating provided by such waves does improve the simulation in the polar winter stratosphere.

Varying the horizontal resolution in the model has provided important insights into the momentum balance of the middle atmosphere. In the early 9°-by-10° horizontal resolution version, the mean zonal wind increases monotonically with height in the middle atmosphere so that the maximum speed is at the top level in the model. In the 5°-by-6° version, on the other hand, the maximum wind speed occurs in jet cores at about 64 km altitude with easterly shear above that level. Thus, the mesospheric polar temperatures deviate substantially from radiative equilibrium. The dependence of the polar temperature profile on horizontal resolution is illustrated in Fig. 11.3. Similarly dramatic changes occur in the zonal wind profile. In

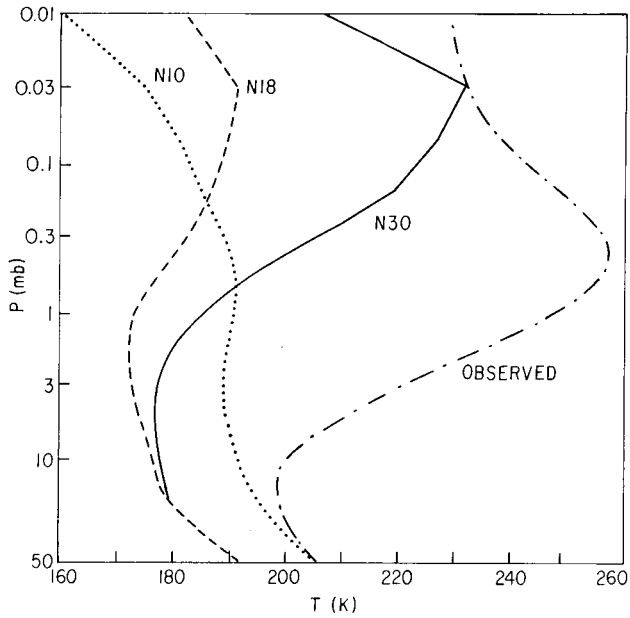

Fig. 11.3. Vertical profiles of the December mean temperature at the north pole simulated by 10°, 5°, and 3° resolution (labeled N10, N18, and N30, respectively) versions of the GFDL SKYHI general circulation model. Chain line shows observed December mean temperature at 80°N from Barnett and Corney (1985a). [Adapted from Fels (1985).]

evaluating the effects of model resolution, it should be noted that the model has a resolution-dependent parameterization of sub-grid-scale diffusion. Thus, in the coarse grid model the planetary waves (which are weaker than observed even in the troposphere) are damped out rapidly in the lower stratosphere; there is little EP flux divergence in the mesosphere, and the mesospheric temperatures are extremely cold. As resolution is improved, the planetary waves penetrate to increasing heights and are dissipated in the mesosphere. The mesospheric temperatures are then greatly improved, but the temperature in the polar stratosphere cools toward radiative equilibrium due to the reduced wave damping there. That planetary wave drag in the mesosphere is important for the 5°-by-6° model is illustrated by the EP flux cross section (Fig. 11.4), which shows a wave drag force of 15 m s^{-1} day^{-1} near the 80-km level. Although this is perhaps only 20% of

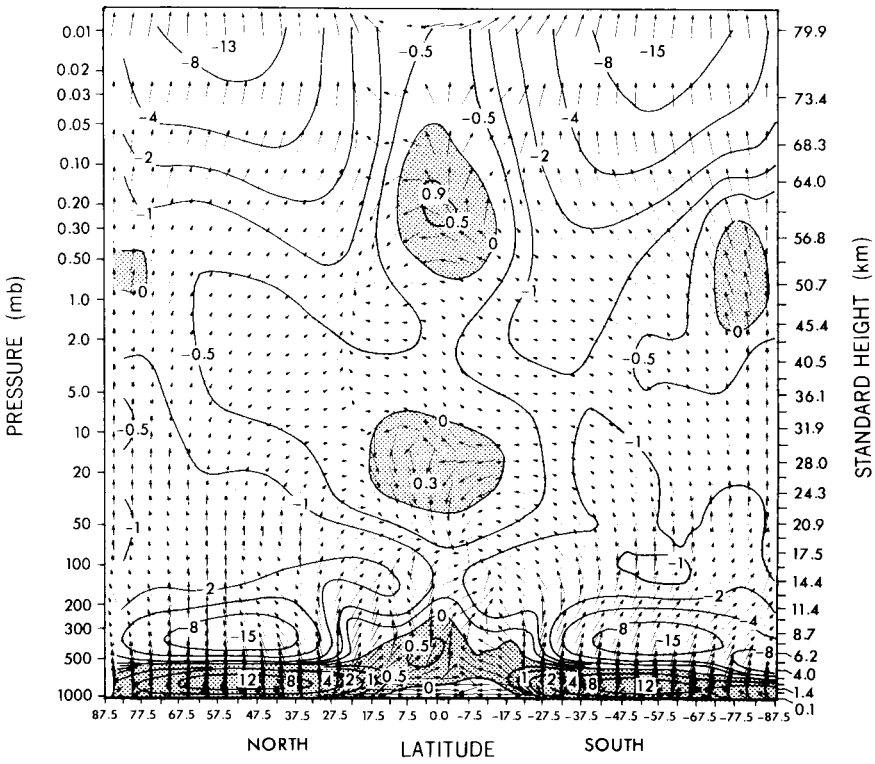

Fig. 11.4. EP flux vector direction (arrows) and contours of EP flux divergence normalized as zonal force per unit mass (10^{-5} m s^{-2}) for a 30-day mean in the SKYHI model with annual mean forcing. [After Andrews *et al.* (1983). American Meteorological Society.]

that required to produce the observed deviation from radiative equilibrium, it is sufficient to produce a substantial deceleration of the winds.

11.2.2 Equatorial Waves

As was indicated in Section 8.5, in its seasonal cycle version the SKYHI model simulates the semiannual oscillation of the zonal winds in the equatorial stratosphere quite realistically. There is little question that the westerly phase of the oscillation in the model, and the atmosphere, is driven by an EP flux divergence associated with upward-propagating equatorial Kelvin waves. A detailed analysis of the equatorial waves simulated in an annual mean 5°-by-6° horizontal resolution version of the SKYHI model is contained in Hayashi *et al.* (1984). In the annual mean simulation, the mean wind is westerly throughout most of the equatorial middle atmosphere and there is, of course, no semiannual oscillation.

A space-time power spectral density plot for the zonal wave-number 1 temperature disturbance in the 5° latitude band centered at the equator is shown in Fig. 11.5. Analysis of the meridional structure confirms that the spectral peaks corresponding to *eastward*-moving waves are indeed Kelvin waves. It is interesting to note that the characteristic period of the waves decreases with increasing height just as found in observations. Thus, the lower stratosphere has waves of period approximately 15 days, in agreement with the observations of Wallace and Kousky (1968). These are damped out below 10 mb. The upper-stratospheric Kelvin waves have periods of 5–7 days (phase speed 60–90 m s^{-1}), while the mesospheric waves have periods of 3–4 days (phase speeds 115–150 m s^{-1}). The corresponding vertical wavelengths are about 10, 20, and 40 km, respectively. These characteristics are in remarkable agreement with the observed waves reported by Salby *et al.* (1984). It is thus not surprising that the model simulates the semiannual oscillation in the upper stratosphere (see Fig. 8.16). However, despite the fact that the model simulates the observed long-period Kelvin waves in the lower stratosphere, there is no evidence of a simulated equatorial quasi-biennial oscillation. This failure is probably due to lack of sufficient vertical resolution. (Recall that the vertical scale of the shear zone in the QBO is only about 2 km.)

In addition to the clear Kelvin wave signal at periods of greater than 2 days, the model also simulates a broad spectrum of short-period equatorial gravity waves that propagate both eastward and westward. These have zonal wave numbers 1–30 and periods of about $\frac{1}{2}$ to 2 days. The contribution of such waves to the momentum balance in the model's middle atmosphere turns out to be at least as large as that of the longer-period Kelvin waves.

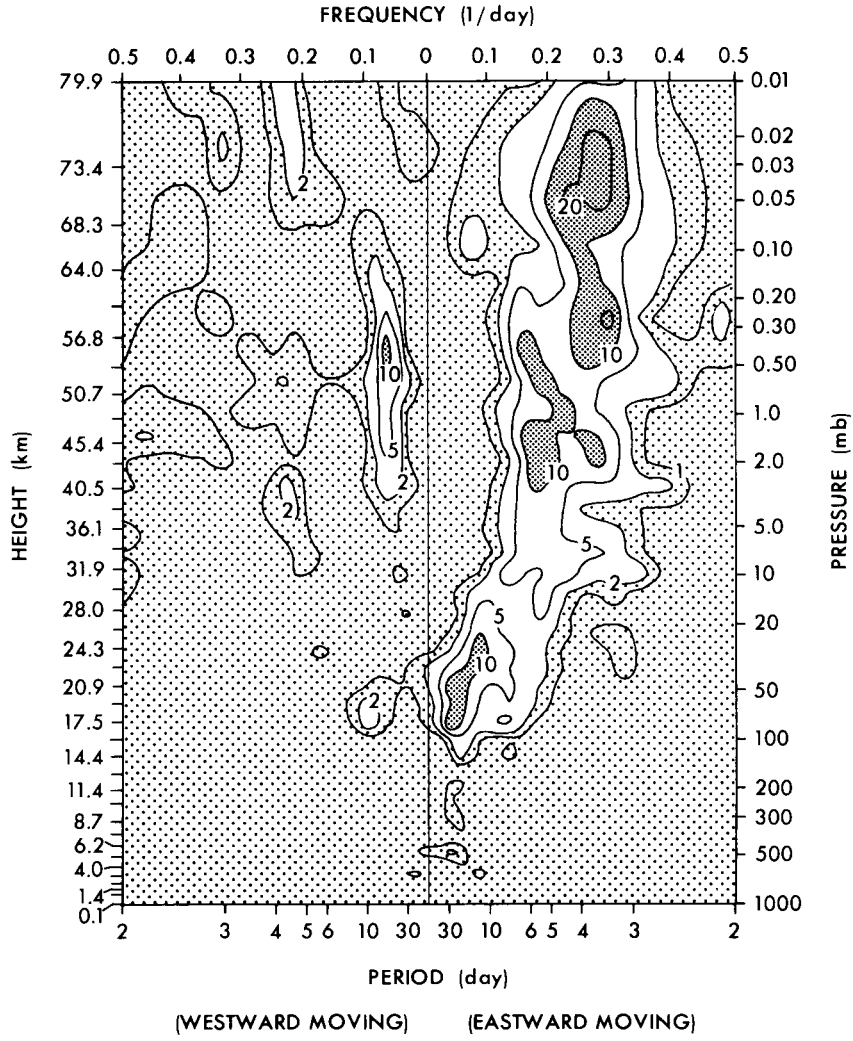

Fig. 11.5. Frequency–height distribution (2.5°S–2.5°N) of space–time power spectral density (K^2 day) of temperature for zonal wave number 1. [After Hayashi *et al.* (1984). American Meteorological Society.]

11.3 Forecasting of Sudden Stratospheric Warmings

There are two basic modes for utilizing a general circulation model: the climate mode, and the forecast mode. In the former mode the model is used to simulate climatological distributions of the atmospheric fields, and the

simulation is validated by comparison with statistics of the observed fields such as time means and variances. In the second mode the model is initialized with real data, and an attempt is made to forecast the evolution of the actual flow over the course of several days.

A number of studies of the dynamics of stratospheric sudden warmings have been carried out using numerical models of varying complexity. Most such investigations have been process-oriented, employing mechanistic models rather than full GCMs; some examples were given in Chapter 6. There have also been studies that have reported sudden warmings generated spontaneously in general circulation models (O'Neill, 1980; Grose and Haggard, 1981; Mahlman and Umscheid, 1984): in all of these examples the models have been run in the climate mode.

The earliest attempt to utilize a GCM to forecast a sudden warming was due to Miyakoda *et al.* (1970). They used a nine-level version of the GFDL model with horizontal grid spacing of about 250 km and the top prediction level at about 9 mb. They attempted to forecast the wave-number 2 final warming of spring 1965 by initializing the model with data from 5 days prior to the observed splitting of the polar vortex. Their forecast did manage to predict the vortex splitting, but the subsequent evolution was not correctly predicted. In the forecast the polar vortex reformed and no vortex breakdown or polar warming occurred. The reasons for the failure of this attempt were not clear at the time. However, it is now known (Simmons and Strüfing, 1983) that the radiation scheme used in this early GFDL model caused much too rapid cooling near the winter pole in the lower stratosphere, and thus tended to rapidly reform the polar vortex. Recent experiments also suggest that a good forecast of the troposphere is a necessary precondition to a successful stratospheric forecast, and the tropospheric forecast in this early experiment was quite poor after a few days.

In recent years the quality of extended-range forecasts has improved dramatically, due both to improved models and to improved initial data. Sudden warmings occurred in January and February 1979, during the Global Weather Experiment (a period of enhanced global observations). Forecasting experiments for this period were carried out by Simmons and Strüfing (1983) and Mechoso *et al.* (1985). Simmons and Strüfing used a modified version of the operational forecast model of the European Centre for Medium Range Weather Forecasts (ECMWF). This model had 18 levels with the top level at 10 mb, and had a horizontal grid spacing of 1.875° in latitude and longitude. A number of 10-day forecasts were carried out for both the January wave-number 1 minor warming and the late-February wave-number 2 major warming. In Fig. 11.6 we show results for 4- and 10-day forecasts initialized on February 13, 1979 (about 5 days prior to vortex splitting). The breakdown of the vortex is forecast quite accurately

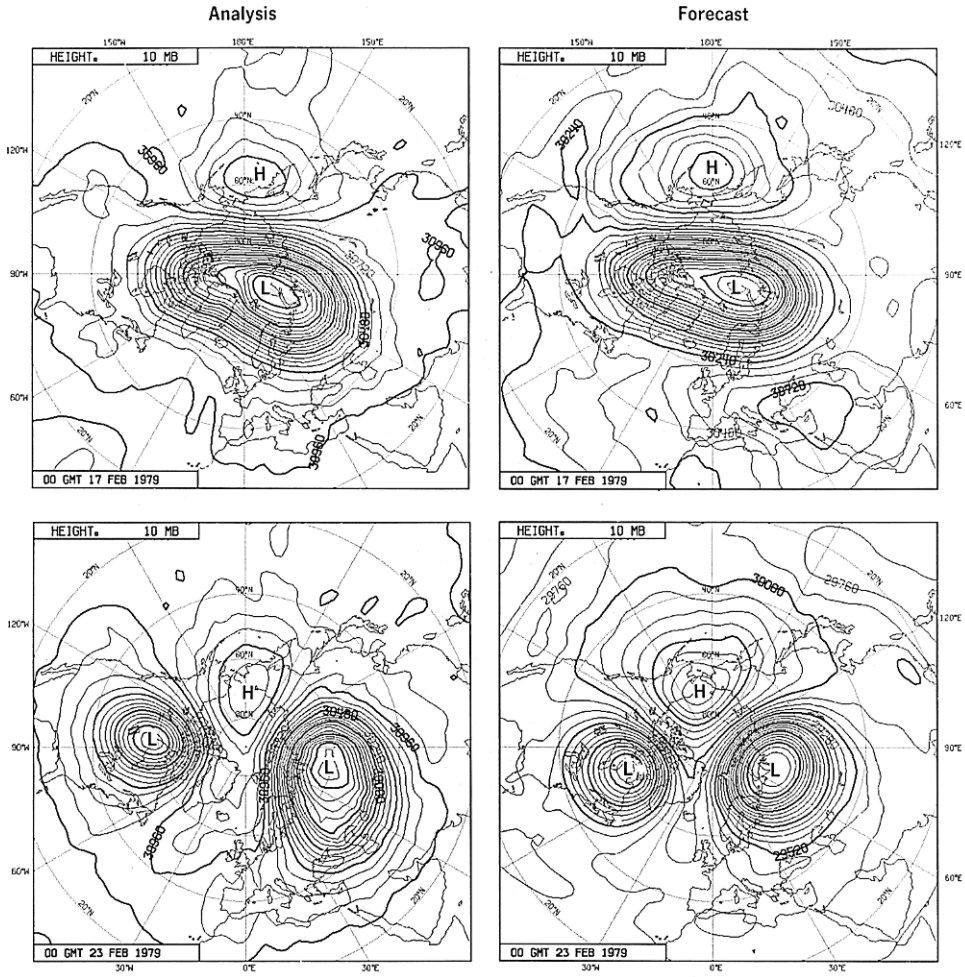

Fig. 11.6. Maps of the 10-mb height for February 17 and 23, 1979 compared with 4- and 10-day forecasts initialized on February 13, 1979. [After Simmons and Strüfing (1983).]

out to 10 days, although the strength of the Aleutian high is somewhat overestimated. Forecasts initialized for other days in this period were also successful, as indicated by the meridional cross sections for several 8-day forecasts shown in Fig. 11.7.

In forecasts of the same sudden warming carried out with a 15-level version of the University of California at Los Angeles (UCLA) general circulation model with an upper boundary at 1 mb, Mechoso *et al.* (1985) found that the influence of horizontal grid resolution was quite important.

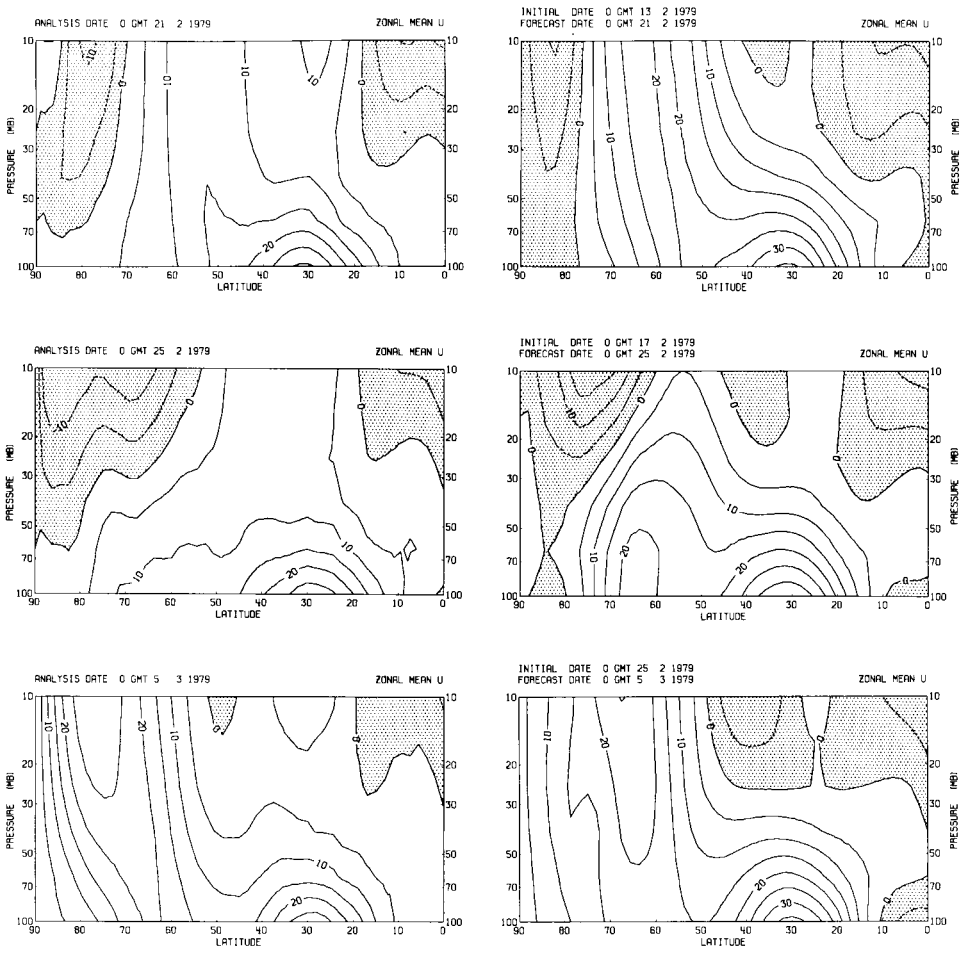

Fig. 11.7. Latitude–height sections of mean zonal winds for February 21, February 25, and March 5, 1979 (left-hand side) and 8-day forecasts verifying for the same dates (right-hand side). [After Simmons and Strüfing (1983).]

They compared forecasts based on a 4° latitude by 5° longitude model with those in a 2.4°-by-3° model. A 10-day forecast with the high-resolution model initialized on February 17, 1979 correctly predicted the vortex breakdown, as shown in Fig. 11.8. The coarse-resolution model predicted substantially less amplification of the wavenumber two pattern. Mechoso *et al.* attributed this difference to the poorer tropospheric forecast in the latter model. In particular, they found that the refractive index squared for wave number 2 (cf. Section 4.5.4) had a negative region in the high-latitude upper

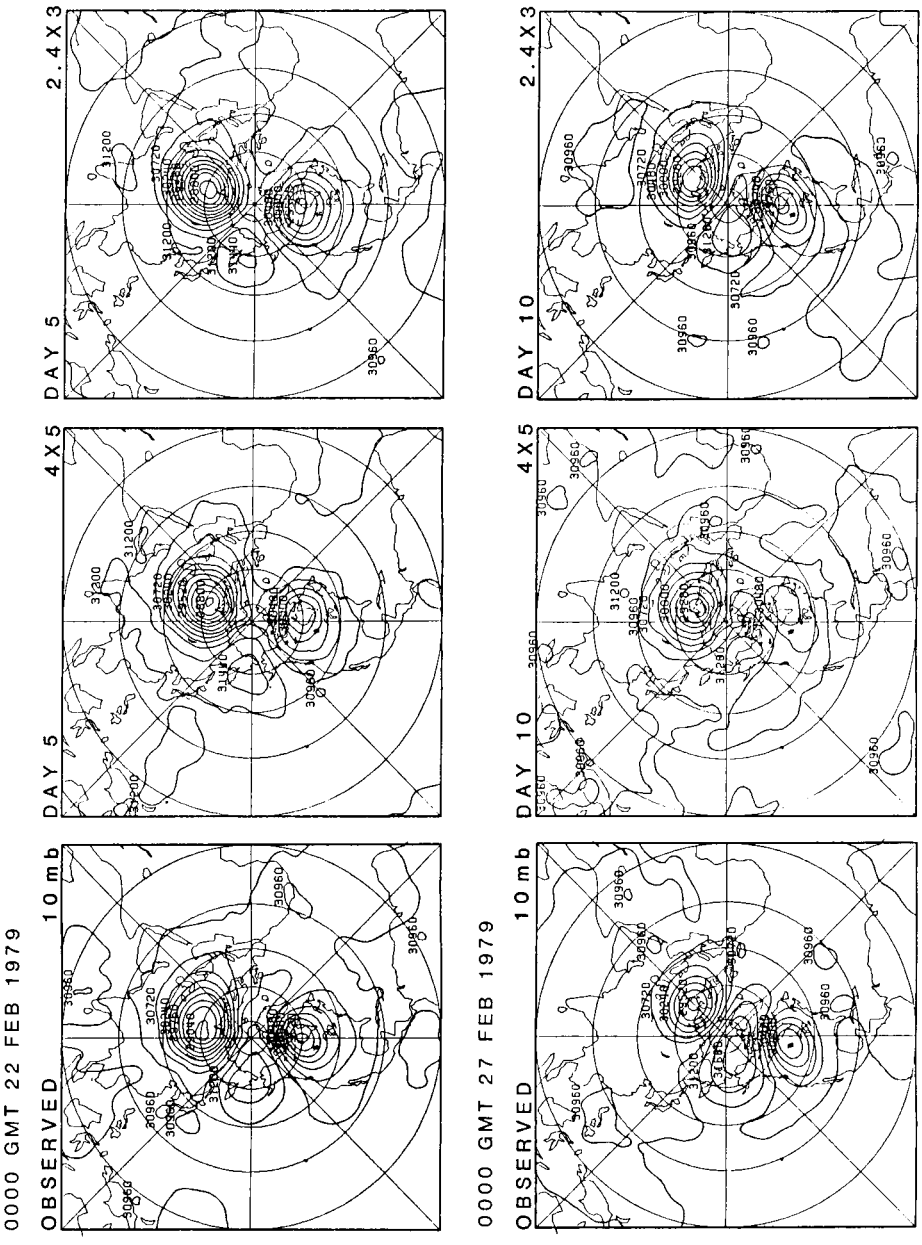

Fig. 11.8. Maps of the 10-mb height observed on February 22 and 27, 1979 and for 5- and 10-day forecasts with the UCLA general circulation model initialized on February 17. [After Mechoso *et al.* (1985). American Meteorological Society.]

troposphere in the low-resolution model that was not present in the high-resolution case. Hence, vertical propagation into the polar stratosphere was underpredicted in the low-resolution model. In conclusion, it appears that, despite the fact that the stratosphere is dominated by planetary scales of motion, a very accurate tropospheric forecast is a minimum requirement for the forecast of a sudden stratospheric warming. Such accuracy depends on many factors, including horizontal resolution.

11.4 Transport Modeling

Simulation of the climatological distribution of ozone and its temporal and spatial variability has long been a goal of middle atmosphere general circulation models. Indeed, the early hemispheric model of Hunt and Manabe (1968) was used by Hunt (1969) to study the influence of transport on ozone in a simulation that included a very simple parameterization of ozone photochemistry. A somewhat more sophisticated treatment of photochemistry was used in a global model by Cunnold *et al.* (1975), but their model was based on the quasi-geostrophic equations and was not a true general circulation model. Schlesinger and Mintz (1979) used the Cunnold *et al.* (1975) photochemistry in a global primitive-equation model with 12 prediction levels, including seven levels in the stratosphere between 100 and 1 mb. The ozone distribution computed in the model was used in the solar radiative heating algorithm. Thus, the model involved feedback among the dynamical, photochemical, and radiative processes. Unfortunately, however, they were unable to integrate the model for a sufficiently long simulated time to establish an equilibrium ozone distribution.

In all of the above studies the tracer (ozone) was carried as an additional dependent scalar variable in the general circulation model. This has the advantage that the calculations for the tracer evolution can be made simply by solving an additional continuity equation to obtain the tracer mixing-ratio distribution at each timestep. If feedback of the tracer onto the dynamics is to be included, this is the only possible strategy. However, for study of the evolution of a *passive* tracer it is rather inefficient to carry the tracer as a variable of the GCM, since each time that a different initial tracer distribution or different photochemical loss rate is tested an entirely new GCM simulation is required. Rather, it is far more efficient to save the winds from the GCM as a "data" set and to solve the tracer continuity equation independently of the GCM using the GCM derived winds as specified advecting velocities. It is this strategy that has been adopted in a number of recent studies of stratospheric tracers carried out at GFDL.

The GFDL tracer model is based on winds obtained from the seasonally varying GFDL global model described by Manabe and Mahlman (1976).

The model has horizontal grid spacing of about 250 km and 11 levels in the vertical arranged to provide good resolution in the boundary layer and in the lower stratosphere. The top level is at 10 mb, so the model is limited to tropospheric and lower-stratospheric tracer studies. However, for many trace species (e.g., ozone) it is the lower stratosphere where transport processes are dominant, while photochemistry controls the distributions at higher altitudes (see Chapter 10). Thus, the model can be used for studying stratospheric transport processes despite the low altitude of the top boundary. The results must be interpreted with caution, however, in view of the cold polar bias in the model.

The details of the tracer model are given by Mahlman and Moxim (1978). Briefly, the model solves a continuity equation for mixing ratio similar to Eq. (9.4.2), but using the terrain-following sigma-coordinate system. In addition to tracer flux divergences due to the explicitly specified winds, the model contains sub-grid-scale horizontal and vertical diffusion, provisions for source and sink terms appropriate to particular tracers, and a "filling" term to eliminate local negative values of mixing ratio that may appear due to finite-differencing truncation errors. The input fields for the tracer model are obtained from an annual cycle run of the GCM in which the wind and surface pressure fields are averaged over 6-hr periods and saved once every 6 hr. The tracer continuity equation is integrated over the annual cycle using a 24-min time step. Additional years of integration can be done by recycling the annually varying wind fields.

Among the studies carried out with this tracer model is a "stratified tracer" experiment (Mahlman *et al.*, 1980) designed to elucidate the role of transport in determining the lower-stratospheric distribution of an ozone-like tracer. For this experiment the tracer mixing ratio was held fixed at 7.5 ppm at the top model level (10 mb) and a simple tracer removal was specified in the troposphere. The tracer was initialized with a horizontally uniform distribution that increased almost linearly with height from the surface to the 10 mb level. The model was integrated over 4 simulated years, which was sufficient to establish an annually varying equilibrium distribution. Results at 3-month intervals for the fourth year are shown in Fig. 11.9. The zonal mean distribution for all seasons shows an upward bulge in the mixing-ratio surfaces in the tropics, and downward slope toward the poles in both hemispheres, consistent with the diabatic circulation of the lower stratosphere discussed in Chapter 9. The poleward-downward slope is greater in the Northern Hemisphere at all seasons, consistent with the model's stronger eddy activity and stronger diabatic circulation in the Northern Hemisphere (Manabe and Mahlman, 1976). A comparison of the terms in the zonal mean tracer budget equations for the northern and southern winters (Fig. 11.10) shows that indeed the eddy tracer fluxes in

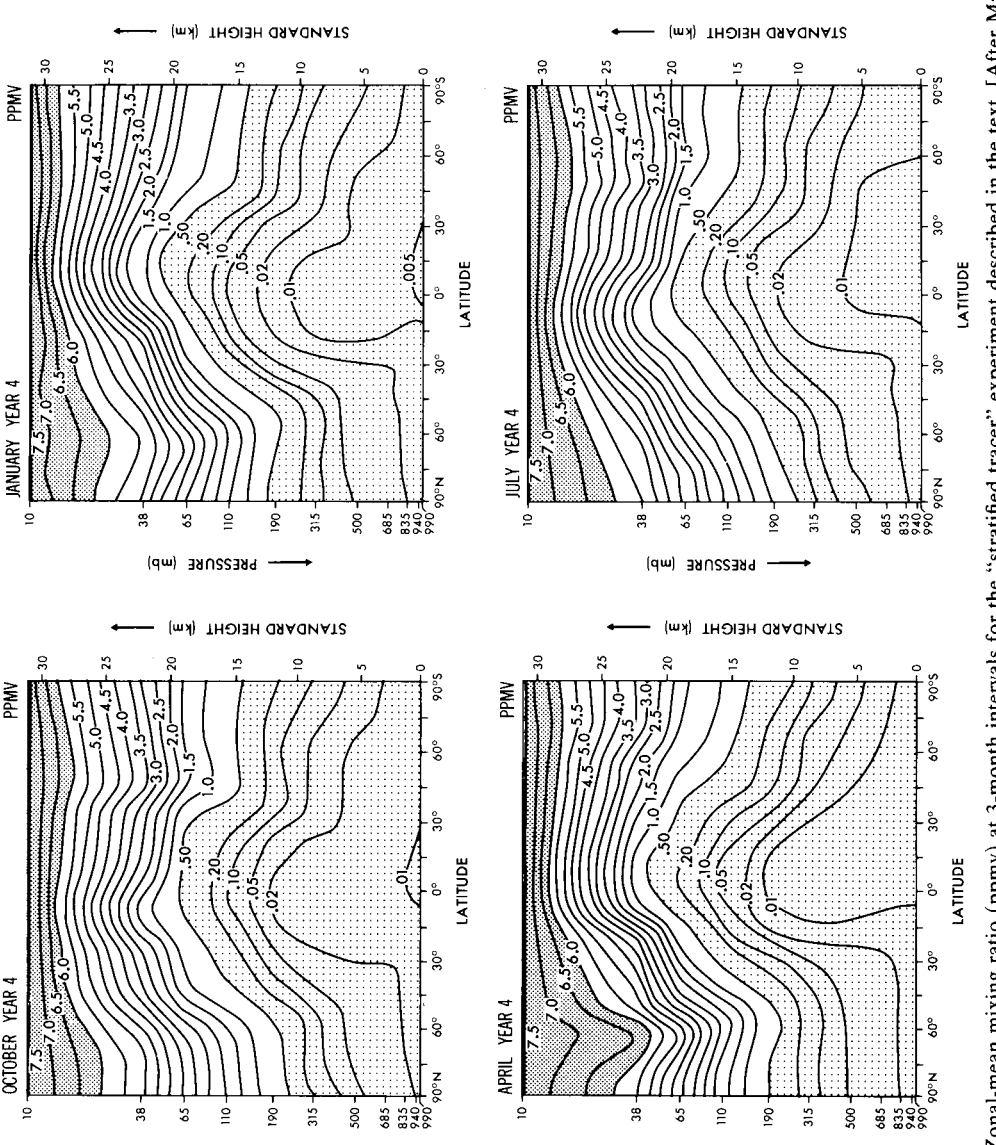

Fig. 11.9. Zonal-mean mixing ratio (ppmv) at 3-month intervals for the "stratified tracer" experiment described in the text. [After Mahlman *et al.* (1980). American Meteorological Society.]

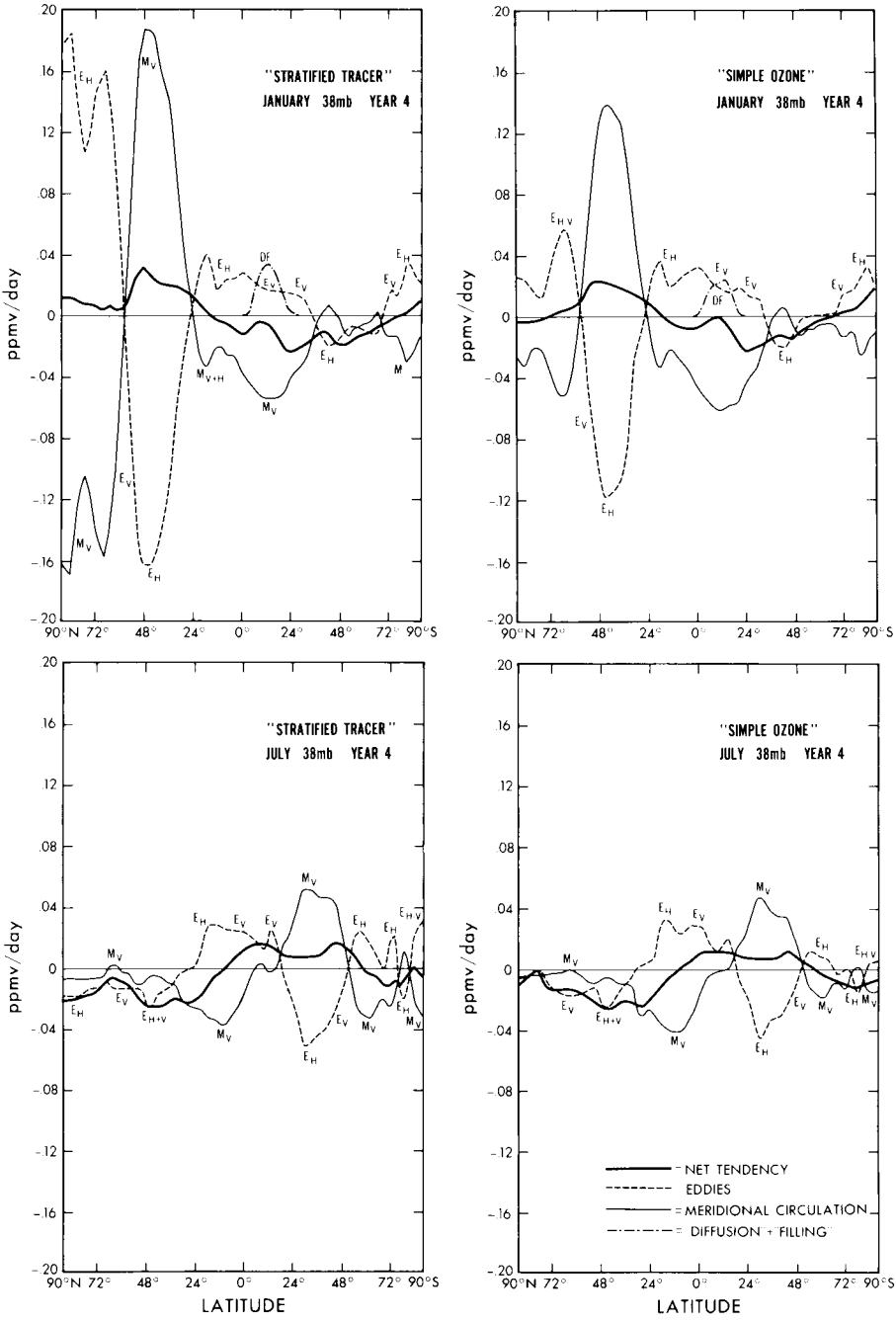

Fig. 11.10. Eulerian-mean balances in the tracer continuity equation at the 38-mb level for two experiments with the GFDL tracer model. [After Mahlman *et al.* (1980). American Meteorological Society.]

the extratropics are much greater in the Northern Hemisphere in January than in the Southern Hemisphere in July.

The Eulerian mean tracer budget of Fig. 11.10 also illustrates the strong compensation between the eddy flux divergence and advection by the mean meridional circulation, which was discussed extensively in Chapter 9. Note especially that near 45°N in January the net tracer tendency is due to a very small excess of mean meridional advection over eddy flux divergence. Thus, conditions in the model at this time and latitude are quite close to those of the nontransport theorem.

In order to better elucidate the net transport, Mahlman *et al.* (1980) used a simple Lagrangian analysis in which they followed short-term isobaric trajectories of a number of parcels advected by the January monthly mean winds from the tracer model. These trajectories show the parcel motions relative to the time mean flow (stationary waves) and do not correspond to the total parcel motions, which depart from isobaric surfaces and are significantly influenced by wave transience (cf. Section 9.4.2). Nevertheless, the schematic parcel drift relative to the mean flow shown in Fig. 11.11

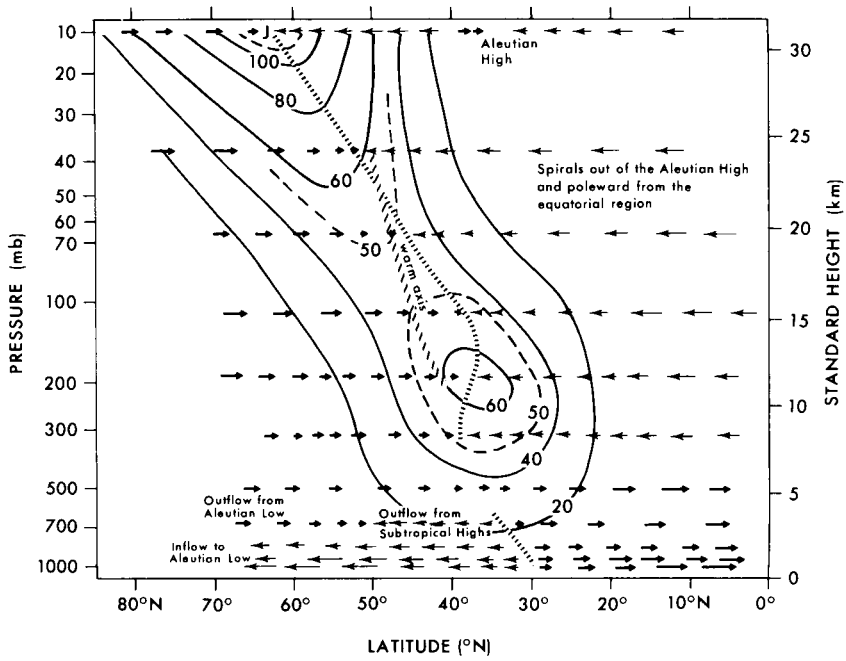

Fig. 11.11. Schematic view of parcel drift relative to the January-mean jetstream simulated in a GCM. Note strong convergence of parcels at and to the poleward side of the time-mean jetstream axis (dashed lines). Diagonal dashed line shows axis of warmest air. [After Mahlman *et al.* (1980). American Meteorological Society.]

should be qualitatively correct. The figure, which shows a cross section at 150°E longitude through the core of the West Pacific jetstream, reveals that the parcel drifts are toward the jetstream core from both the equatorial and polar sides. The effect of this parcel drift is to intensify the gradient of the tracer across the jet (Fig. 11.12) by poleward advection of low mixing ratios and equatorward advection of high mixing ratios. Comparison of Fig. 11.12 with Fig. 9.12 indicates that the parcel drifts in the model are attempting to produce a tracer distribution similar to that of the observed ozone distribution associated with a folded tropopause. The limited horizontal and vertical resolution in the model prevents formation of an actual fold. Nevertheless, it is clear that the model is able to simulate the large-scale environment required for formation of tropopause folds.

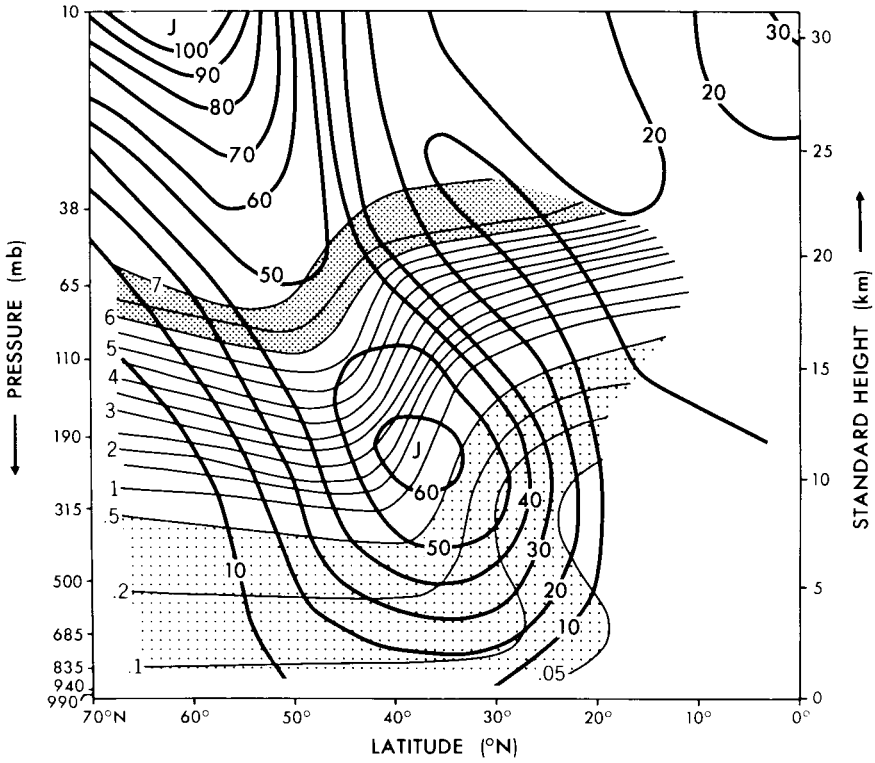

Fig. 11.12. January-mean mixing ratio calculated relative to the simulated jetstream at 150°E for the stratified tracer experiment described in the text. Note the downward displacement of high values on the poleward side of the jet. [After Mahlman *et al.* (1980). American Meteorological Society.]

The stratified tracer experiment represents a study of a stratospheric source gas (i.e., a tracer that is produced in the stratosphere and is transported to the troposphere, where it is destroyed). Another important class of tracers are the long-lived tropospheric source gases, which are produced in the troposphere and destroyed in the stratosphere; some typical vertical profiles of such tracers were shown in Fig. 1.8. The GFDL tracer model has been used by Mahlman *et al.* (1986) to study the transport of a representative tropospheric source gas (N_2O). They examined the dependence of the mean tracer distribution on the chemical timescale, by running simulations with three differing assumed rates of stratospheric destruction. The "slow-sink" case, whose January monthly mean meridional cross section is shown in Fig. 11.13, represents the best estimate of the actual atmospheric destruction rates, with a vertical profile of chemical lifetime similar to that of Fig. 9.2. The general pattern in Fig. 11.13 is in agreement with observations (cf. Fig. 9.3); the model simulates the familiar poleward-downward slopes of the constant-mixing-ratio surfaces, with slopes very similar to those of the stratified tracer experiment shown in Fig. 11.9. However, in the model, unlike the atmosphere, the equatorial bulge remains centered south of the equator for almost the entire year.

The major differences apparent between the slow sink and a "fast-sink" simulation (with chemical lifetimes about half those in the slow sink case) are in the meridional and vertical gradients, which are much steeper in the fast sink case. The meridional tracer slope,

$$\left(\frac{\partial z}{\partial y}\right)_{\bar{\chi}=\text{constant}} = -\bar{\chi}_y/\bar{\chi}_z, \tag{11.4.1}$$

is, however, nearly the same for the two cases. This similarity of equilibrium slopes is typical of all tracers for which the chemical timescale is long relative to the transport timescale. The similarity of slopes also extends to the longitudinal direction. Thus, the topography of time-mean mixing ratio surfaces is similar for all long-lived tracers. Comparison of the model with observations of N_2O shows that the meridional slopes in the model are about 30% smaller than the observed slopes. Mahlman *et al.* argue that this discrepancy is due to the fact that the eddies in the model stratosphere are not as active as in the real atmosphere, and hence the diabatic circulation is underestimated. This defect is, of course, directly related to the polar cold bias of the GCM discussed in Section 11.2.

Global data from satellite observations are available for only a very limited number of tracers. Thus, comparisons of model simulated global distributions with observed distributions are not always possible. Some comparisons can still be made, however, by using the time series of "data"

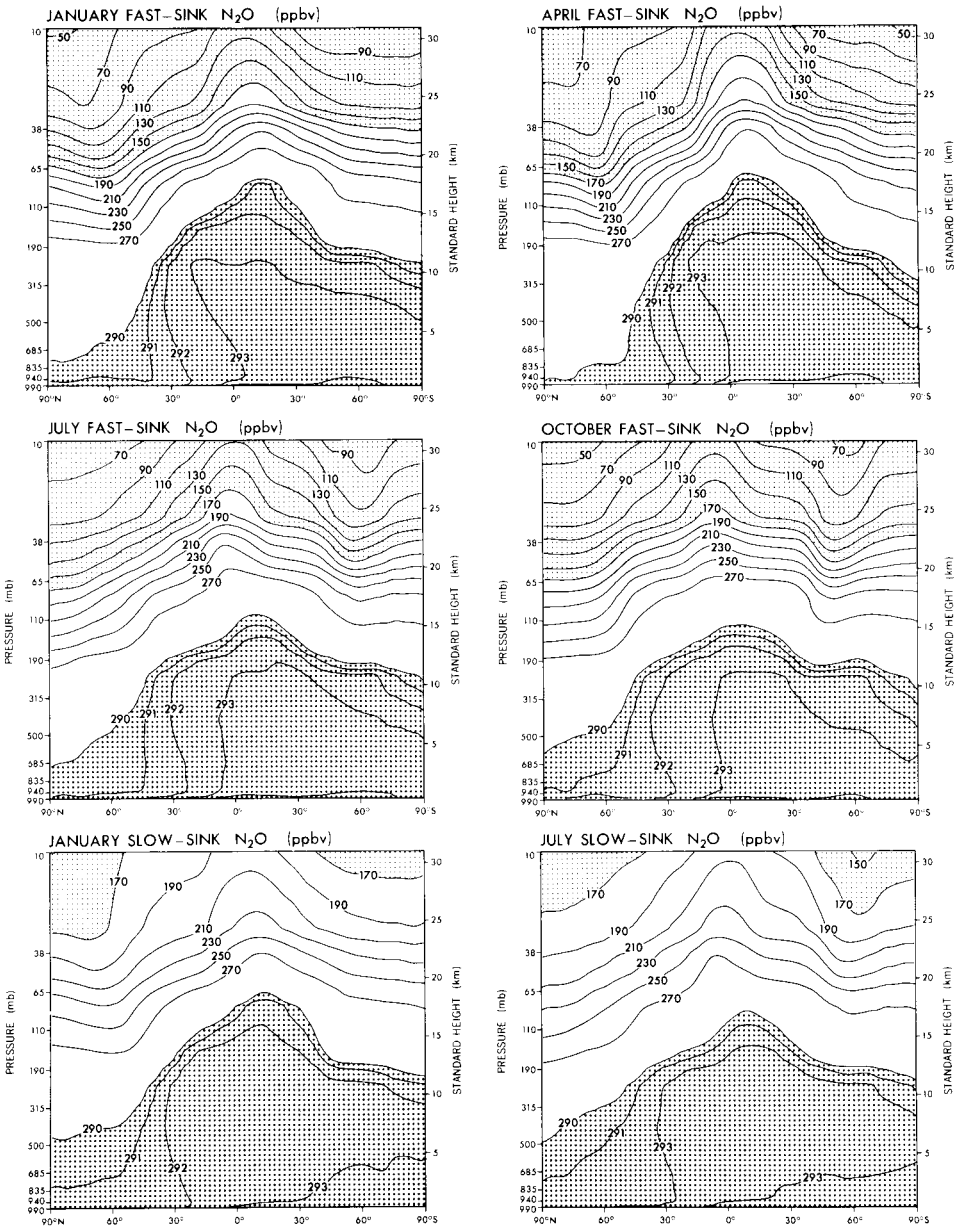

Fig. 11.13. Height-latitude distribution of simulated N_2O in the GFDL tracer model. [After Mahlman *et al.* (1986).]

generated at a particular grid location in the model to compare the temporal variability of the simulated tracer with that found in long series of observations. Mahlman *et al.* (1986) evaluated the "equivalent displacement height" defined in Eq. (9.5.2) for their N_2O simulation using the grid point nearest Laramie, Wyoming, a location for which there are a number of balloon-borne tracer measurements. The vertical profiles from the model and from the observations (shown in Fig. 11.14) are remarkably similar, indicating that the model does produce about the right amount of temporal variance. Synoptic maps of the N_2O distribution simulated in the model reveal that large pulses of temporal variability can be accounted for by rapid meridional transport associated with planetary wavebreaking, just as in the cases of observed ozone, methane, and potential vorticity discussed in Chapter 9.

The GFDL tracer model has demonstrated that three-dimensional general circulation models are powerful tools for the study of tracer transport. As these models become increasingly sophisticated, it should be possible to use them to simulate the annually varying ozone distribution with accurate photochemical and radiative heating algorithms and thus to achieve a primary goal for middle atmosphere science: a completely coupled radiative, dynamical, and photochemical model.

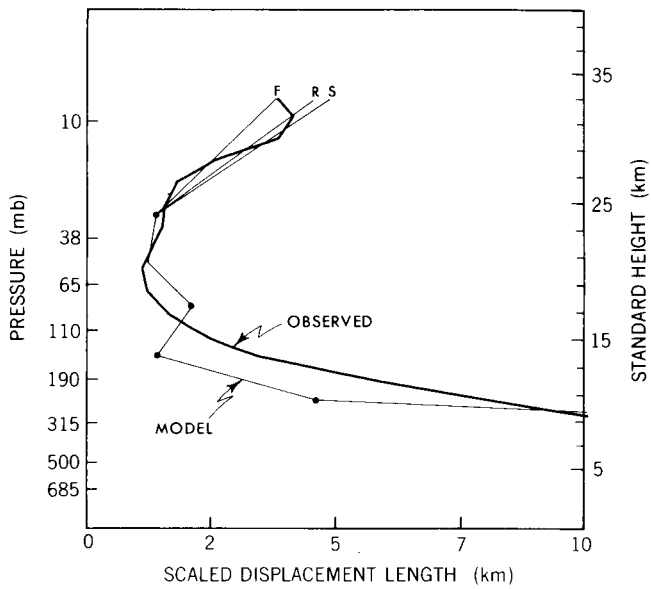

Fig. 11.14. Vertical profiles of equivalent displacement heights for N_2O simulated in the GFDL tracer model compared to observed values for Laramie, Wyoming. [After Mahlman *et al.* (1986).]

References

11.1. A review of models of the middle atmospheric circulation is given by Geller (1984). Haltiner and Williams (1980) provide a nice survey of the various numerical techniques and physical parameterizations used in GCMs. General circulation modeling by spectral methods is reviewed by Bourke *et al.* (1977). A stratospheric GCM developed at the United Kingdom Meteorological Office is described by O'Neill *et al.* (1982).

11.2. The basic structure of the GFDL models is discussed in Holloway and Manabe (1971). Results from these models are given in a number of papers, including Manabe and Terpstra (1974) Manabe *et al.* (1974), and Manabe and Mahlman (1976). For the SKYHI model, see Fels *et al.* (1980), Mahlman and Umscheid (1984), and Miyahara *et al.* (1986).

11.3. Initialization of global models for real data forecasts is reviewed by Daley (1981). The ECMWF forecast model is described by Burridge and Haseler (1977).

11.4. The interpretation of tracer transport experiments in isobaric and isentropic coordinates is discussed by Mahlman (1985). A detailed analysis of water-vapor transport in a GCM is given in Allam and Tuck (1984).